Centrum voor Wiskunde en Informatica
REPORT*RAPPORT*

Note on PARNASSOS, a Navier-Stokes method for ship-stern flows

B. Koren

Modelling, Analysis and Simulation (MAS)

MAS-R9808 June 30, 1998

Report MAS-R9808
ISSN 1386-3703

CWI
P.O. Box 94079
1090 GB Amsterdam
The Netherlands

Note on PARNASSOS, a Navier-Stokes Method for Ship-Stern Flows

Barry Koren
CWI
P.O. Box 94079, 1090 GB Amsterdam, The Netherlands

ABSTRACT
In this report, analyses are made of some of the numerical techniques implemented in MARIN's viscous ship-hydrodynamics software PARNASSOS. Suggestions are given to improve the robustness of PARNASSOS and – where appropriate – its accuracy and computational efficiency. The effects to be expected from some of the proposed modifications are analyzed as well.

1991 Mathematics Subject Classification: 35B05, 35B35, 35M10, 65N06, 65N12, 76D05, 76M20.
Keywords and Phrases: ship hydrodynamics, reduced Navier-Stokes equations, qualitative solution behavior, grid types, finite differences, accuracy, monotonicity, stability.
Note: This work was performed under a research contract with the Maritime Research Institute Netherlands and was carried out under CWI-project MAS2.1 "Computational Fluid Dynamics".

1. Introduction

1.1 PARNASSOS

The flow equations considered in PARNASSOS are the steady, 3D, incompressible, Reynolds-averaged Navier-Stokes equations with free-surface effects neglected and – also – all diffusion terms in mainstream direction. Near the ship, the mainstream direction is assumed to be tangential to the hull. The resulting reduced Navier-Stokes equations yield a reliable flow model for attached, thin boundary-layer flow along infinitely long geometries (i.e., geometries without leading and trailing edges). In case of separation, the equations may lose their validity. PARNASSOS is mainly used for flow-topology studies near ship sterns. (An important first objective of ship designers is to get an impression of the local flow field the propeller has to operate in.) Since separation is to be expected most in the ship-stern region, care has to be taken in interpreting computational results. The fact that the stern is a trailing edge causes no problems. For a flat plate, it is known that at high Reynolds numbers, the flow model near the trailing edge has a triple-deck structure [13], where in the lower of the three decks the full Navier-Stokes equations must be applied ([2], p. 230–232 and [3], p. 4,12,18,22). Fortunately, because of the very high Reynolds numbers in ship hydrodynamics, the sizes of this full-Navier-Stokes deck are negligible in practice.

The equations are discretized in computational space. The discretization uses finite differences on a non-staggered grid. The resulting residuals, though, are staggered. The solution method for the discretized equations exploits the fact that, due to the absence of diffusion in one direction, the equations are mixed parabolic-elliptic. The parabolic part dominates the elliptic. Therefore, parabolic solution methods (marching methods) are appropriate. As a result of the remaining ellipticity of the equations, a single-march method only is insufficient. The solver has to be equipped for the elliptic part, which contains the pressure derivatives. To solve for the pressure, use can be made of well-established techniques such as the pseudo-compressibility [1] or the pressure-correction method [6]. The authors of PARNASSOS have chosen for an interesting alternative: pressure relaxation via the momentum equation in mainstream direction. We refrain from a further description of PARNASSOS and refer to publications by its authors. For an overview, see [8], for more detailed descriptions, see [9, 10, 11].

1.2 Problem description

The kind of computational domain in which PARNASSOS is applied, is sketched in Figure 1. In here, the shaded curvilinear plane represents the hull of a half ship's rear part. The piece of hull extends from the stern to about halfway the ship's length. It forms part of the computational domain's boundary of which the remainder is the symmetry plane at $y = 0$. At the other boundaries, that in the $(z = 0)$-plane is a symmetry boundary as well. Those in the planes $x = 0$ and $x = x_{\max}$ are inflow and outflow boundaries, respectively. The inflow conditions near the hull are derived from a boundary-layer solution. Further away, a potential-flow solution is employed to determine the inflow conditions. (In the farfield, the potential flow is in x-direction.) At the remaining, curvilinear outer boundary (Figure 1), the conditions imposed follow from the potential-flow solution only.

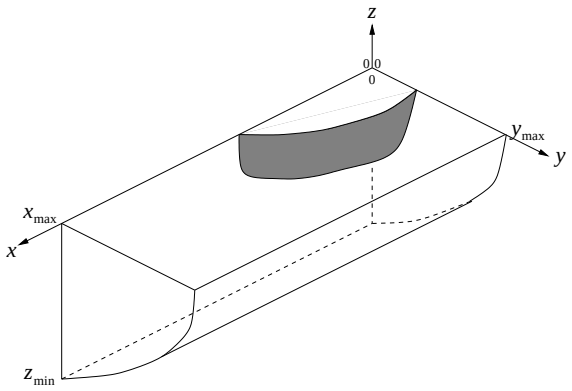

Figure 1: Sketch of computational domain considered in PARNASSOS.

For the discretization of the computational domain, an HO-type grid is applied. At the $(z = 0)$-boundary, the grid plane is of H-type (Figure 2a). The density of grid lines running in mainstream direction is highest in the boundary-layer flow along the hull. Although this is suggested in Figure 2a, the grid is not necessarily normal to the ship's symmetry plane. Instead, it may very well be normal to the ship hull. At the inflow and outflow boundaries, the grid planes are of O-type (Figure 2b). The grid plane at the outflow boundary (lower sketch in Figure 2b) is singular; the most inner circumferential grid line has an infinitely large curvature in its lowest point $z = z_{\text{singular}}$. The radial grid line through $z = z_{\text{singular}}$ suffers infinite curvature as well. (In the singular point, each of the two grid lines is *both* at a finite angle *and* tangential to the $(y = 0)$-plane.) The grid singularity does not only occur at the most downstream grid plane, it is present in all grid planes downstream of the stern. The singularity has its origin at the lower part of the ship stern. An unfavorable circumstance is that this is in the region of interest, where the propeller is placed. In computational practice, the grid singularity appears to result in robustness problems. The aim of this work is to find a fix for these robustness problems.

1.3 Solution approach and outline of report

To solve the grid-singularity problem, the obvious way seems to be the generation of a non-singular grid. However, sticking to the same type of grid, the remedies may also be sought in, e.g., a discretization with better stability properties, or in a solver with better convergence properties. Seeking in a broader context may yield a fix which is simpler and as effective as that of the construction of a regular grid. In this report, we will follow this more general approach. In Section 2, the reduced Navier-Stokes model considered in PARNASSOS is analyzed with respect to the type of partial differential equations and the qualitative solution behavior. In Section 3, the existing numerical techniques that have been incorporated in PARNASSOS are analyzed to some extent: some numerical properties of the difference formulae and some properties of the pressure relaxation (the less standard part of

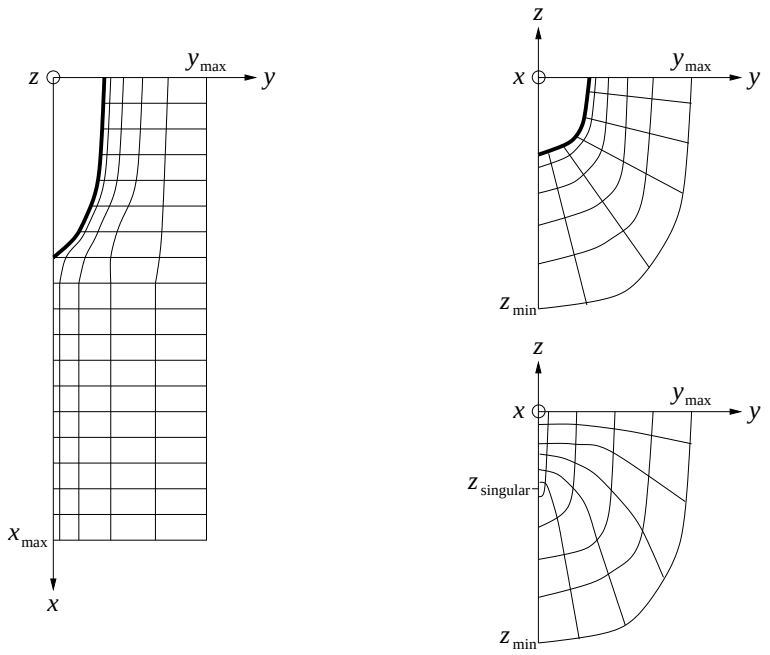

a. H-type grid plane at $z = 0$.

b. O-type grid planes, at $x = 0$ (above) and at $x = x_{\max}$ (below).

Figure 2: Sketches of grid planes.

the solution method) are studied. Partially based on the results of Section 3, in Sections 4, 5 and 6, some modifications of the numerical method are proposed and – where possible – analyzed. The modifications are classified as not promising (Section 4), somewhat promising (Section 5) and promising (Section 6). In this report, no numerical results are presented.

2. Continuous equations

Let us consider a Cartesian coordinate system x, y, z and let us assume that the x-direction is the mainstream direction. Then, the flow equations considered in PARNASSOS can be written as

$$\frac{\partial u}{\partial x} + \frac{\partial v}{\partial y} + \frac{\partial w}{\partial z} = 0, \tag{2.1a}$$

$$u\frac{\partial u}{\partial x} + v\frac{\partial u}{\partial y} + w\frac{\partial u}{\partial z} + \frac{\partial p}{\partial x} - \frac{1}{\mathrm{Re}}\left(\frac{\partial^2 u}{\partial y^2} + \frac{\partial^2 u}{\partial z^2}\right) = 0, \tag{2.1b}$$

$$u\frac{\partial v}{\partial x} + v\frac{\partial v}{\partial y} + w\frac{\partial v}{\partial z} + \frac{\partial p}{\partial y} - \frac{1}{\mathrm{Re}}\left(\frac{\partial^2 v}{\partial y^2} + \frac{\partial^2 v}{\partial z^2}\right) = 0, \tag{2.1c}$$

$$u\frac{\partial w}{\partial x} + v\frac{\partial w}{\partial y} + w\frac{\partial w}{\partial z} + \frac{\partial p}{\partial z} - \frac{1}{\mathrm{Re}}\left(\frac{\partial^2 w}{\partial y^2} + \frac{\partial^2 w}{\partial z^2}\right) = 0, \tag{2.1d}$$

where the density is supposed to be embodied in p and the turbulence model in Re. In the practice of PARNASSOS, a curvilinear coordinate system is considered, fitted to the ship hull. It is in this

curvilinear system that a mainstream direction is assigned, i.e., the direction in which all diffusion terms are neglected. Thus, Cartesian, reduced Navier-Stokes system (2.1) is no valid flow model for strongly curvilinear geometries, only for rectilinear such as that sketched in Figure 3, it may be so. For first analysis purposes, we think that system (2.1) is to be preferred above a curvilinear one. It yields more transparent results.

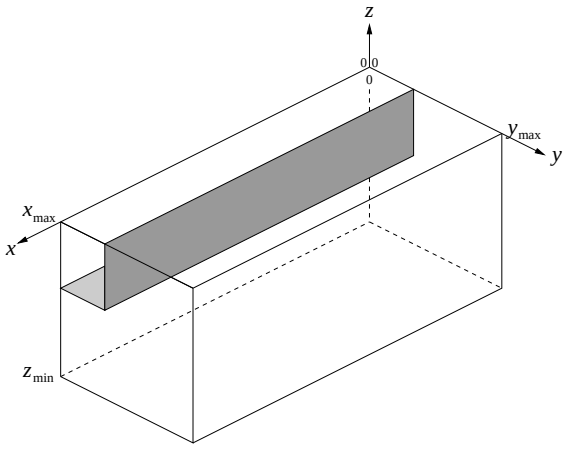

Figure 3: Infinitely long, half flat-plate hull, with computational domain.

2.1 Type of equations

To investigate the type of the equations, we rewrite the system operator in (2.1) to the corresponding higher-order, scalar operator. For this purpose, assume the non-constant coefficients u, v, w and, in case of turbulence, also $\frac{1}{\mathrm{Re}}$ to be frozen and rewrite (2.1) in the matrix form

$$\begin{pmatrix} \frac{\partial}{\partial x} & \frac{\partial}{\partial y} & \frac{\partial}{\partial z} & 0 \\ \alpha & 0 & 0 & \frac{\partial}{\partial x} \\ 0 & \alpha & 0 & \frac{\partial}{\partial y} \\ 0 & 0 & \alpha & \frac{\partial}{\partial z} \end{pmatrix} \begin{pmatrix} u \\ v \\ w \\ p \end{pmatrix} = \begin{pmatrix} 0 \\ 0 \\ 0 \\ 0 \end{pmatrix}, \quad \alpha = \overline{u}\frac{\partial}{\partial x} + \overline{v}\frac{\partial}{\partial y} + \overline{w}\frac{\partial}{\partial z} - \frac{1}{\overline{\mathrm{Re}}}\left(\frac{\partial^2}{\partial y^2} + \frac{\partial^2}{\partial z^2}\right), \tag{2.2}$$

where the frozen coefficients have been overlined. The corresponding scalar operator is given by the determinant of above matrix, i.e., by

$$\left(\frac{\partial^2}{\partial x^2} + \frac{\partial^2}{\partial y^2} + \frac{\partial^2}{\partial z^2}\right)\left[\overline{u}\frac{\partial}{\partial x} + \overline{v}\frac{\partial}{\partial y} + \overline{w}\frac{\partial}{\partial z} - \frac{1}{\overline{\mathrm{Re}}}\left(\frac{\partial^2}{\partial y^2} + \frac{\partial^2}{\partial z^2}\right)\right]^2. \tag{2.3}$$

We see that the determinant is the product of two differential operators, the first is elliptic, the second is parabolic (in x-direction). Given the quadratic form of the latter operator, the complete operator is predominantly parabolic. To compare, the full Navier-Stokes equations are purely elliptic; the corresponding determinant yields the sixth-order elliptic operator $\left(\frac{\partial^2}{\partial x^2} + \frac{\partial^2}{\partial y^2} + \frac{\partial^2}{\partial z^2}\right)\left[\overline{u}\frac{\partial}{\partial x} + \overline{v}\frac{\partial}{\partial y} + \overline{w}\frac{\partial}{\partial z} - \frac{1}{\overline{\mathrm{Re}}}\left(\frac{\partial^2}{\partial x^2} + \frac{\partial^2}{\partial y^2} + \frac{\partial^2}{\partial z^2}\right)\right]^2$. The second-order ellipticity, which is still present in (2.3), originates from the velocity derivatives in the continuity equation and from the pressure derivatives. Elimination in (2.2) of these derivatives, leads to $\left[\overline{u}\frac{\partial}{\partial x} + \overline{v}\frac{\partial}{\partial y} + \overline{w}\frac{\partial}{\partial z} - \frac{1}{\overline{\mathrm{Re}}}\left(\frac{\partial^2}{\partial y^2} + \frac{\partial^2}{\partial z^2}\right)\right]^3$, which is purely parabolic indeed. With the knowledge that system (2.1) is second-order elliptic and fourth-order parabolic, from existing theory on the well-posedness of boundary-value problems, it is known that the numbers of

boundary conditions that have to be imposed in this case are: one at outflow in x-direction and three at all other boundaries. (Given the knowledge that the second-order elliptic nature is partly due to the pressure derivatives, it seems natural that for the single outflow condition a pressure condition is taken.) In the next section, the qualitative solution behavior will be investigated. There, it will be derived that the numbers of boundary conditions mentioned here are indeed necessary to get a well-posed problem.

2.2 Qualitative solution behavior

Before investigating the solution behavior of the reduced Navier-Stokes system (2.1), we first analyze the full Navier-Stokes system. For both systems of equations, it is assumed that the solution can be written as the complex Fourier series

$$\begin{pmatrix} u \\ v \\ w \\ p \end{pmatrix} = \frac{1}{(2\pi)^3} \sum_{m=-\infty}^{\infty} \sum_{l=-\infty}^{\infty} \sum_{k=-\infty}^{\infty} \begin{pmatrix} \hat{u} \\ \hat{v} \\ \hat{w} \\ \hat{p} \end{pmatrix}_{k,l,m} e^{\mathrm{i}(\omega_x)_k x} e^{\mathrm{i}(\omega_y)_l y} e^{\mathrm{i}(\omega_z)_m z}. \tag{2.4}$$

Linearizing the two systems of Navier-Stokes equations by freezing (as in Section 2.1) the non-constant coefficients u, v, w and possibly $\frac{1}{\mathrm{Re}}$, we only need to consider a single Fourier component. Let us write this component as

$$\begin{pmatrix} u \\ v \\ w \\ p \end{pmatrix} = \begin{pmatrix} U \\ V \\ W \\ P \end{pmatrix} e^{\mathrm{i}\omega_x x} e^{\mathrm{i}\omega_y y} e^{\mathrm{i}\omega_z z}, \tag{2.5}$$

and the linearized coefficients again as $\overline{u}, \overline{v}, \overline{w}$ and $\frac{1}{\overline{\mathrm{Re}}}$.

Full Navier-Stokes equations. Substitution of (2.5) into the linearized, full Navier-Stokes equations yields

$$\begin{pmatrix} \mathrm{i}\omega_x & \mathrm{i}\omega_y & \mathrm{i}\omega_z & 0 \\ \beta & 0 & 0 & \mathrm{i}\omega_x \\ 0 & \beta & 0 & \mathrm{i}\omega_y \\ 0 & 0 & \beta & \mathrm{i}\omega_z \end{pmatrix} \begin{pmatrix} u \\ v \\ w \\ p \end{pmatrix} = \begin{pmatrix} 0 \\ 0 \\ 0 \\ 0 \end{pmatrix}, \quad \beta = \mathrm{i}\left(\overline{u}\omega_x + \overline{v}\omega_y + \overline{w}\omega_z\right) + \frac{1}{\overline{\mathrm{Re}}}\left(\omega_x^2 + \omega_y^2 + \omega_z^2\right). \tag{2.6}$$

A non-trivial solution of (2.6) exists if the determinant of the matrix in (2.6) equals zero, i.e., if

$$\left(\omega_x^2 + \omega_y^2 + \omega_z^2\right)\left[\mathrm{i}\left(\overline{u}\omega_x + \overline{v}\omega_y + \overline{w}\omega_z\right) + \frac{1}{\overline{\mathrm{Re}}}\left(\omega_x^2 + \omega_y^2 + \omega_z^2\right)\right]^2 = 0. \tag{2.7}$$

We proceed by looking for the solution modes ω_x of (2.7). From the first factor, it directly follows the two solutions

$$(\omega_x)_{1,2} = \pm\mathrm{i}\sqrt{\omega_y^2 + \omega_z^2}. \tag{2.8a}$$

The solutions ω_x from the second factor can be directly written out as well. To keep the analysis transparent, the latter solutions are expanded in terms of the small parameter $\frac{1}{\mathrm{Re}}$, yielding

$$(\omega_x)_{3,4} = -\left(\frac{\overline{v}}{\overline{u}}\omega_y + \frac{\overline{w}}{\overline{u}}\omega_z\right) + \mathrm{i}\frac{(\overline{v}\omega_y + \overline{w}\omega_z)^2 + \overline{u}^2(\omega_y^2 + \omega_z^2)}{\overline{u}^3}\frac{1}{\overline{\mathrm{Re}}} + \mathcal{O}\left(\frac{1}{\overline{\mathrm{Re}}^2}\right), \tag{2.8b}$$

$$(\omega_x)_{5,6} = -\mathrm{i}\overline{u}\overline{\mathrm{Re}} + \left(\frac{\overline{v}}{\overline{u}}\omega_y + \frac{\overline{w}}{\overline{u}}\omega_z\right) - \mathrm{i}\frac{(\overline{v}\omega_y + \overline{w}\omega_z)^2 + \overline{u}^2(\omega_y^2+\omega_z^2)}{\overline{u}^3}\frac{1}{\overline{\mathrm{Re}}} + \mathcal{O}\left(\frac{1}{\overline{\mathrm{Re}}^2}\right). \tag{2.8c}$$

Both are double roots because the second factor is squared. In analyzing $(\omega_x)_1, \ldots, (\omega_x)_6$, we assume that ω_y and ω_z are real. Then, the root $(\omega_x)_1 = +\mathrm{i}\sqrt{\omega_y^2+\omega_z^2}$ implies exponential decrease of the solution in positive x-direction and exponential increase in negative x-direction. For $(\omega_x)_2$, the opposite holds. In $(\omega_x)_{3,4}$, the $\mathcal{O}(1)$-term implies a neutrally stable, oscillating solution behavior. The $\mathcal{O}(\frac{1}{\overline{\mathrm{Re}}})$-term in $(\omega_x)_{3,4}$ on its turn, implies damping in positive x-direction and growth in the opposite direction, for $\overline{u} > 0$. For $\overline{u} < 0$, the behavior is the reverse. Hence, the combined effect of the $\mathcal{O}(1)$- and the $\mathcal{O}(\frac{1}{\overline{\mathrm{Re}}})$-term in $(\omega_x)_{3,4}$ is an oscillatory solution that diminishes and grows exponentially in downstream and upstream direction, respectively. Finally, the double root $(\omega_x)_{5,6}$ implies a solution behavior which is exactly the opposite of that of $(\omega_x)_{3,4}$. In Table 1, the solution behavior in x-direction is summarized. The minus signs define solution decrease and the plus signs increase. Because of the similarity of equation (2.7) with respect to ω_x, ω_y and ω_z, for the y- and z-directions, the tables corresponding to Table 1 are similar. (The tables for the y- and z-direction can be directly obtained from Table 1 by replacing $x, \overline{u}, (\omega_x)_{1-6}$ by $y, \overline{v}, (\omega_y)_{1,\ldots,6}$ and $z, \overline{w}, (\omega_z)_{1,\ldots,6}$, respectively.)

	$x \to +\infty$		$x \to -\infty$	
	$\overline{u} > 0$	$\overline{u} < 0$	$\overline{u} > 0$	$\overline{u} < 0$
$(\omega_x)_1$	$-$	$-$	$+$	$+$
$(\omega_x)_2$	$+$	$+$	$-$	$-$
$(\omega_x)_3$	$-$	$+$	$+$	$-$
$(\omega_x)_4$	$-$	$+$	$+$	$-$
$(\omega_x)_5$	$+$	$-$	$-$	$+$
$(\omega_x)_6$	$+$	$-$	$-$	$+$

Table 1: Qualitative solution behavior of full Navier-Stokes equations, in a single coordinate direction, $+$ means solution increase, $-$ solution decrease.

For each of the four possible $(x, \overline{u})$-cases in Table 1, three exponentially growing solution modes appear (three plus signs per column). The same holds for the y- and z-direction. Hence, to ensure a stable solution, in each coordinate direction, independent of the sign of the (frozen) velocity component, three conditions must be imposed at each of the two corresponding boundaries.

Reduced Navier-Stokes equations. Substitution of (2.5) into the linearized, reduced Navier-Stokes equations (2.1) yields

$$\begin{pmatrix} \mathrm{i}\omega_x & \mathrm{i}\omega_y & \mathrm{i}\omega_z & 0 \\ \gamma & 0 & 0 & \mathrm{i}\omega_x \\ 0 & \gamma & 0 & \mathrm{i}\omega_y \\ 0 & 0 & \gamma & \mathrm{i}\omega_z \end{pmatrix} \begin{pmatrix} u \\ v \\ w \\ p \end{pmatrix} = \begin{pmatrix} 0 \\ 0 \\ 0 \\ 0 \end{pmatrix}, \quad \gamma = \mathrm{i}\left(\overline{u}\omega_x + \overline{v}\omega_y + \overline{w}\omega_z\right) + \frac{1}{\overline{\mathrm{Re}}}\left(\omega_y^2+\omega_z^2\right). \tag{2.9}$$

Setting the determinant of the matrix in (2.9) equal to zero, gives for the Fourier modes ω_x, ω_y and ω_z the equation

$$\left(\omega_x^2+\omega_y^2+\omega_z^2\right)\left[\mathrm{i}\left(\overline{u}\omega_x + \overline{v}\omega_y + \overline{w}\omega_z\right) + \frac{1}{\overline{\mathrm{Re}}}\left(\omega_y^2+\omega_z^2\right)\right]^2 = 0. \tag{2.10}$$

Now, the corresponding, exact solutions ω_x are

$$(\omega_x)_{1,2} = \pm \mathrm{i}\sqrt{\omega_y^2 + \omega_z^2}, \tag{2.11a}$$

$$(\omega_x)_{3,4} = -\left(\frac{\overline{v}}{\overline{u}}\omega_y + \frac{\overline{w}}{\overline{u}}\omega_z\right) + \mathrm{i}\frac{\omega_y^2 + \omega_z^2}{\overline{u}}\frac{1}{\overline{\mathrm{Re}}}. \tag{2.11b}$$

The roots $(\omega_x)_{1,2}$ are identical to those for full Navier-Stokes. The double root $(\omega_x)_{3,4}$ differs in form, but implies the same solution behavior as that for full Navier-Stokes: exponential diminution in flow direction and exponential growth in upstream direction. The qualitative solution behavior is summarized in Table 2.

	$x \to +\infty$		$x \to -\infty$	
	$\overline{u} > 0$	$\overline{u} < 0$	$\overline{u} > 0$	$\overline{u} < 0$
$(\omega_x)_1$	$-$	$-$	$+$	$+$
$(\omega_x)_2$	$+$	$+$	$-$	$-$
$(\omega_x)_3$	$-$	$+$	$+$	$-$
$(\omega_x)_4$	$-$	$+$	$+$	$-$

Table 2: Qualitative solution behavior of reduced Navier-Stokes equations, in mainstream direction, $+$ means solution increase, $-$ solution decrease.

Hence, for the reduced Navier-Stokes equations, it follows that to obtain a stable solution in mainstream direction (here the x-direction), three boundary conditions must be imposed at inflow and one at outflow. In the two other directions (here the y- and z-direction), it can be easily verified that, just as for full Navier-Stokes, three conditions must be imposed at each of the boundaries.

In PARNASSOS, the above numbers of boundary conditions are imposed at all boundaries, with the exception of the $(y = 0)$-symmetry boundary and the $(z = 0)$-symmetry boundary (the water surface). There, instead of three, four conditions are imposed, viz. $\frac{\partial u}{\partial y} = 0, v = 0, \frac{\partial w}{\partial y} = 0, \frac{\partial p}{\partial y} = 0$ at the $(y = 0)$-symmetry boundary and $\frac{\partial u}{\partial z} = 0, \frac{\partial v}{\partial z} = 0, w = 0, \frac{\partial p}{\partial z} = 0$ at the water surface. This seems to be inconsistent overspecification; substitution of the conditions $v(x, z) = 0$ and $w(x, y) = 0$ into the corresponding momentum equation normal to the two boundaries yields $\frac{\partial p}{\partial y} = \frac{1}{\mathrm{Re}}\frac{\partial^2 v}{\partial y^2}$ and $\frac{\partial p}{\partial z} = \frac{1}{\mathrm{Re}}\frac{\partial^2 w}{\partial z^2}$, respectively. In the "real" double-hull case, at $y = 0$ and $z = 0$, it will hold $\frac{\partial^2 v}{\partial y^2} = 0$ and $\frac{\partial^2 w}{\partial z^2} = 0$, respectively. So, the overspecification *is* consistent.

3. Analysis of existing numerical method

For reasons of transparency, the numerical analysis is not done for the 3D discrete reduced Navier-Stokes equations, but for the 2D discrete case at most. So, as the continuous starting equations we take

$$\frac{\partial u}{\partial x} + \frac{\partial v}{\partial y} = 0, \tag{3.1a}$$

$$u\frac{\partial u}{\partial x} + v\frac{\partial u}{\partial y} + \frac{\partial p}{\partial x} - \frac{1}{\mathrm{Re}}\frac{\partial^2 u}{\partial y^2} = 0, \tag{3.1b}$$

$$u\frac{\partial v}{\partial x} + v\frac{\partial v}{\partial y} + \frac{\partial p}{\partial y} - \frac{1}{\mathrm{Re}}\frac{\partial^2 v}{\partial y^2} = 0. \tag{3.1c}$$

Taking into account the parabolic-elliptic nature of the reduced Navier-Stokes equations, in PARNASSOS, all first-order x-derivatives are discretized by three-point backward difference formulae, with the exception of the (elliptic) pressure derivative $\frac{\partial p}{\partial x}$, which is discretized downstream. All other derivatives in (3.1) are discretized by central difference formulae. Noteworthy is that the discretization is done staggered in y-direction. I.e., when the discretization of the x-momentum equation is done in grid point i, j, where i denotes the grid point number in x-direction and j that in y-direction, then the continuity equation is discretized in point $i, j-\frac{1}{2}$ and the y-momentum equation in point $i, j+\frac{1}{2}$. Considering an equidistant grid with mesh sizes $\Delta x = \Delta y = h$, in PARNASSOS, the discretization of system (3.1) would then be

$$\frac{1}{2}\left(\frac{3u_{i,j-1} - 4u_{i-1,j-1} + u_{i-2,j-1}}{2h} + \frac{3u_{i,j} - 4u_{i-1,j} + u_{i-2,j}}{2h}\right) + \frac{v_{i,j} - v_{i,j-1}}{h} = 0, \tag{3.2a}$$

$$u_{i,j}\frac{3u_{i,j} - 4u_{i-1,j} + u_{i-2,j}}{2h} + v_{i,j}\frac{u_{i,j+1} - u_{i,j-1}}{2h} + \frac{p_{i+1,j} - p_{i,j}}{h} - \frac{1}{\mathrm{Re}}\frac{u_{i,j+1} - 2u_{i,j} + u_{i,j-1}}{h^2} = 0, \tag{3.2b}$$

$$\frac{u_{i,j} + u_{i,j+1}}{2}\frac{1}{2}\left(\frac{3v_{i,j} - 4v_{i-1,j} + v_{i-2,j}}{2h} + \frac{3v_{i,j+1} - 4v_{i-1,j+1} + v_{i-2,j+1}}{2h}\right) + \frac{v_{i,j} + v_{i,j+1}}{2}\frac{v_{i,j+1} - v_{i,j}}{h} + \frac{p_{i,j+1} - p_{i,j}}{h} - \frac{1}{\mathrm{Re}}\frac{1}{2}\left(\frac{v_{i,j+1} - 2v_{i,j} + v_{i,j-1}}{h^2} + \frac{v_{i,j+2} - 2v_{i,j+1} + v_{i,j}}{h^2}\right) = 0. \tag{3.2c}$$

3.1 Accuracy

Through Taylor-series expansions around grid point i, j, from (3.2), the following system of modified equations is found

$$\left(1 - \frac{h}{2}\frac{\partial}{\partial y}\right)\left(\frac{\partial u}{\partial x} + \frac{\partial v}{\partial y}\right) = \mathcal{O}(h^2), \tag{3.3a}$$

$$u\frac{\partial u}{\partial x} + v\frac{\partial u}{\partial y} + \frac{\partial p}{\partial x} - \frac{1}{\mathrm{Re}}\frac{\partial^2 u}{\partial y^2} = -\frac{h}{2}\frac{\partial^2 p}{\partial x^2} + \mathcal{O}(h^2), \tag{3.3b}$$

$$\left(1 + \frac{h}{2}\frac{\partial}{\partial y}\right)\left(u\frac{\partial v}{\partial x} + v\frac{\partial v}{\partial y} + \frac{\partial p}{\partial y} - \frac{1}{\mathrm{Re}}\frac{\partial^2 v}{\partial y^2}\right) = \mathcal{O}(h^2). \tag{3.3c}$$

So, the discretization of the continuity and y-momentum equation is $\mathcal{O}(h^2)$-accurate, but that of the x-momentum equation is $\mathcal{O}(h)$-accurate, and therefore, through the coupling of the equations, the discretization of the whole system is $\mathcal{O}(h)$-accurate. The system is kept from full $\mathcal{O}(h^2)$-accuracy by the $\mathcal{O}(h)$-discretization of $\frac{\partial p}{\partial x}$ only.

3.2 Monotonicity

Neglecting the partially elliptic nature of the flow equations, as well as the nonlinearity, a further simplified, but still representative model equation of the reduced 3D Navier-Stokes equations (2.1) is the stripped-off boundary-layer equation

$$\overline{u}\frac{\partial u}{\partial x} - \frac{1}{\overline{\mathrm{Re}}}\frac{\partial^2 u}{\partial y^2} = 0, \quad \overline{u} > 0. \tag{3.4}$$

Considering again an equidistant grid with $\Delta x = \Delta y = h$, in PARNASSOS, the discretization of (3.4) would be

$$\overline{u}\frac{3u_{i,j} - 4u_{i-1,j} + u_{i-2,j}}{2h} - \frac{1}{\overline{\mathrm{Re}}}\frac{u_{i,j+1} - 2u_{i,j} + u_{i,j-1}}{h^2} = 0, \quad \overline{u} > 0, \tag{3.5}$$

from which it follows

$$u_{i,j} = \frac{4u_{i-1,j} - u_{i-2,j} + \frac{2}{\overline{u}\overline{\mathrm{Re}}h}\left(u_{i,j+1} + u_{i,j-1}\right)}{3 + \frac{4}{\overline{u}\overline{\mathrm{Re}}h}}, \quad \overline{u} > 0. \tag{3.6}$$

The coefficient of $u_{i-2,j}$ is negative. Hence, an increase or decrease of $u_{i-2,j}$ will always lead to a decrease or increase, respectively, of $u_{i,j}$, and thus to possible spurious non-monotonicities in the numerical solution. Note that because the three-point backward difference formula is applied to all first-order velocity derivatives in mainstream direction, the above non-positivity is present in all discrete equations. It is assumed, though, that the flow solution is in general sufficiently smooth in mainstream direction so that non-physical solution oscillations are not to be expected. Since the three-point backward difference formula is not self-starting, care has to be taken that no non-smoothness is introduced in the first marching step.

3.3 Stability

Marching with the parabolic part. In this section we will continue by analyzing the stability properties of a downstream marching method applied to (3.5). In text books, it can be read that stability is guaranteed indeed for the specific discretization at hand, and – furthermore – that it is unconditional (see, e.g., [12], p. 190). Since we do not know books in which the unconditional stability is really shown, for completeness, we will do so here. For this purpose, consider again an equidistant grid with $\Delta x = \Delta y = h$ and introduce the discrete Fourier-series component

$$u_{i,j} = U\rho^i e^{\mathrm{i}\theta_2 j}, \quad -\pi \le \theta_2 \equiv \omega_2 h \le \pi, \tag{3.7}$$

where ρ is the amplification factor sought for. Substitution of (3.7) into (3.5) yields the following quadratic equation for ρ

$$\overline{u}\frac{3 - \frac{4}{\rho} + \frac{1}{\rho^2}}{2h} - \frac{1}{\overline{\mathrm{Re}}}\frac{e^{\mathrm{i}\theta_2} - 2 + e^{-\mathrm{i}\theta_2}}{h^2} = 0, \quad \overline{u} > 0, \tag{3.8}$$

from which it follows

$$\rho_{1,2} = \frac{2 \pm \sqrt{1-\alpha}}{3+\alpha}, \quad \alpha = \frac{8}{\overline{u}\overline{\mathrm{Re}}h}\sin^2\left(\frac{\theta_2}{2}\right), \quad \overline{u} > 0. \tag{3.9}$$

The stability requirements are: $-1 \le \rho_{1,2} \le 1$, for any value of the mesh Reynolds number $\overline{\mathrm{Re}}h$ and for any grid mode θ_2. The requirement $\rho_{1,2} \le 1$ translates into $\alpha \ge -3$, which, given $\overline{u} > 0$, is always satisfied. The requirement $\rho_{1,2} \ge -1$ boils down to $(\alpha+5)^2 \ge 1-\alpha$, which is also satisfied without any constraints, given $\overline{u} > 0$. This confirms the stability of the downstream marching method for the discrete parabolic part.

Relaxation of the elliptic part. The pressure relaxation is done through the momentum equation in mainstream direction. In PARNASSOS, both downstream and upstream relaxation sweeps are applied. In this report, downstream relaxation sweeps will be looked at only. (This will yield a reasonable amount of information from which first conclusions can be drawn.) The model system considered is (3.2) with the coefficients in the nonlinear terms frozen, yielding three free parameters:

$\overline{u}, \overline{v}$ and $\overline{\mathrm{Re}}h$. By introducing the superscript n as the counter for the relaxation sweeps, the discrete equations to be considered then, are

$$\frac{1}{4}\left[\left(3u^n_{i,j-1} - 4u^n_{i-1,j-1} + u^n_{i-2,j-1}\right) + \left(3u^n_{i,j} - 4u^n_{i-1,j} + u^n_{i-2,j}\right)\right] + \left(v^n_{i,j} - v^n_{i,j-1}\right) = 0, \quad (3.10a)$$

$$\frac{1}{2}\overline{u}\left(3u^n_{i,j} - 4u^n_{i-1,j} + u^n_{i-2,j}\right) + \frac{1}{2}\overline{v}\left(u^n_{i,j+1} - u^n_{i,j-1}\right) + \left(p^{n-1}_{i+1,j} - p^n_{i,j}\right) - \frac{1}{\overline{\mathrm{Re}}h}\left(u^n_{i,j+1} - 2u^n_{i,j} + u^n_{i,j-1}\right) = 0, \quad (3.10b)$$

$$\frac{1}{4}\overline{u}\left[\left(3v^n_{i,j} - 4v^n_{i-1,j} + v^n_{i-2,j}\right) + \left(3v^n_{i,j+1} - 4v^n_{i-1,j+1} + v^n_{i-2,j+1}\right)\right] + \overline{v}\left(v^n_{i,j+1} - v^n_{i,j}\right) + \left(p^n_{i,j+1} - p^n_{i,j}\right) - \frac{1}{2}\frac{1}{\overline{\mathrm{Re}}h}\left[\left(v^n_{i,j+1} - 2v^n_{i,j} + v^n_{i,j-1}\right) + \left(v^n_{i,j+2} - 2v^n_{i,j+1} + v^n_{i,j}\right)\right] = 0. \quad (3.10c)$$

To analyze the convergence properties of the pressure relaxation, we introduce the following Fourier form for the local solution

$$q_{i,j} = \begin{pmatrix} u \\ v \\ p \end{pmatrix}_{i,j} = \begin{pmatrix} U \\ V \\ P \end{pmatrix} e^{\mathrm{i}\theta_1 i} e^{\mathrm{i}\theta_2 j}, \quad -\pi \le \theta_1 \equiv \omega_1 h \le \pi, \quad -\pi \le \theta_2 \equiv \omega_2 h \le \pi. \quad (3.11)$$

Then, the pressure relaxation can be rewritten as

$$\tilde{L}q^n_{i,j} = \tilde{L}q^{n-1}_{i,j} - Lq^{n-1}_{i,j}, \quad \text{with} \quad (3.12a)$$

$$L = \begin{pmatrix} \frac{1}{4}\left(3 - 4e^{-\mathrm{i}\theta_1} + e^{-2\mathrm{i}\theta_1}\right)\left(1 + e^{-\mathrm{i}\theta_2}\right) & 1 - e^{-\mathrm{i}\theta_2} & 0 \\ \frac{1}{2}\overline{u}\left(3 - 4e^{-\mathrm{i}\theta_1} + e^{-2\mathrm{i}\theta_1}\right) + \frac{1}{2}\overline{v}\left(e^{\mathrm{i}\theta_2} - e^{-\mathrm{i}\theta_2}\right) - \frac{1}{\overline{\mathrm{Re}}h}\left(e^{\mathrm{i}\theta_2} - 2 + e^{-\mathrm{i}\theta_2}\right) & 0 & e^{\mathrm{i}\theta_1} - 1 \\ 0 & \frac{1}{4}\overline{u}\left(3 - 4e^{-\mathrm{i}\theta_1} + e^{-2\mathrm{i}\theta_1}\right)\left(e^{\mathrm{i}\theta_2} + 1\right) + \overline{v}\left(e^{\mathrm{i}\theta_2} - 1\right) - \frac{1}{2}\frac{1}{\overline{\mathrm{Re}}h}\left(e^{\mathrm{i}\theta_2} - 2 + e^{-\mathrm{i}\theta_2}\right)\left(e^{\mathrm{i}\theta_2} + 1\right) & e^{\mathrm{i}\theta_2} - 1 \end{pmatrix} \quad \text{and} \quad (3.12b)$$

$$\tilde{L} = L - \begin{pmatrix} 0 & 0 & 0 \\ 0 & 0 & e^{\mathrm{i}\theta_1} \\ 0 & 0 & 0 \end{pmatrix}. \quad (3.12c)$$

In here, in Fourier form, L is the target operator to be solved and $\tilde{L}$ the approximate operator to be inverted. Note that $\tilde{L}$ is very close to L. The amplification matrix of the pressure relaxation is defined as

$$M = \tilde{L}^{-1}\left(\tilde{L} - L\right). \quad (3.13)$$

Its three eigenvalues determine the convergence properties of the pressure relaxation. Thanks to the close resemblance of $\tilde{L}$ and L, two of the three eigenvalues ρ of M equal zero:

$$\rho_1 = \rho_2 = 0, \quad \rho_3 = \frac{e^{\mathrm{i}\theta_1}\tilde{L}_{1,1}\tilde{L}_{3,2}}{\tilde{L}_{1,1}\tilde{L}_{3,2} - \tilde{L}_{1,2}\tilde{L}_{2,1}\tilde{L}_{3,3}}, \quad (3.14)$$

with the $\tilde{L}_{i,j}$'s the matrix elements of $\tilde{L}$. As long as $\tilde{L}$ is so close to L that we know in advance that only a single eigenvalue of the corresponding amplification matrix is non-zero, in the remainder of this paper, for the pressure relaxation's convergence analysis, instead of (3.11), we can also directly make the following Ansatz:

$$\begin{pmatrix} u \\ v \\ p \end{pmatrix}^n_{i,j} = \begin{pmatrix} U \\ V \\ P \end{pmatrix} \rho^n e^{\mathrm{i}\theta_1 i} e^{\mathrm{i}\theta_2 j}, \quad -\pi \leq \theta_1 \equiv \omega_1 h \leq \pi, \quad -\pi \leq \theta_2 \equiv \omega_2 h \leq \pi, \tag{3.15}$$

with ρ denoting the amplification factor. Substitution of (3.15) into (3.10) yields

$$\begin{pmatrix} \frac{1}{4}\left(3-4e^{-\mathrm{i}\theta_1}+e^{-2\mathrm{i}\theta_1}\right)\left(1+e^{-\mathrm{i}\theta_2}\right) & 1-e^{-\mathrm{i}\theta_2} & 0 \\ \frac{1}{2}\overline{u}\left(3-4e^{-\mathrm{i}\theta_1}+e^{-2\mathrm{i}\theta_1}\right)+ \frac{1}{2}\overline{v}\left(e^{\mathrm{i}\theta_2}-e^{-\mathrm{i}\theta_2}\right)- \frac{1}{\mathrm{Re}h}\left(e^{\mathrm{i}\theta_2}-2+e^{-\mathrm{i}\theta_2}\right) & 0 & \frac{1}{\rho}e^{\mathrm{i}\theta_1}-1 \\ 0 & \frac{1}{4}\overline{u}\left(3-4e^{-\mathrm{i}\theta_1}+e^{-2\mathrm{i}\theta_1}\right)\left(e^{\mathrm{i}\theta_2}+1\right)+ \overline{v}\left(e^{\mathrm{i}\theta_2}-1\right)- \frac{1}{2}\frac{1}{\mathrm{Re}h}\left(e^{\mathrm{i}\theta_2}-2+e^{-\mathrm{i}\theta_2}\right)\left(e^{\mathrm{i}\theta_2}+1\right) & e^{\mathrm{i}\theta_2}-1 \end{pmatrix} \begin{pmatrix} u \\ v \\ p \end{pmatrix}^n_{i,j} = \begin{pmatrix} 0 \\ 0 \\ 0 \end{pmatrix}. \tag{3.16}$$

Note that the matrix in (3.16), say A, is related to the foregoing matrix L as

$$A = L + \begin{pmatrix} 0 & 0 & 0 \\ 0 & 0 & \left(\frac{1}{\rho}-1\right)e^{\mathrm{i}\theta_1} \\ 0 & 0 & 0 \end{pmatrix}. \tag{3.17}$$

An expression for the amplification factor ρ can be directly derived from (3.16) by setting the determinant of the matrix equal to zero. Here, it appears that the resolvability of ρ depends on the being non-zero of the matrix element corresponding with the $\frac{\partial u}{\partial x}$-term from the continuity equation and the one belonging to the derivatives of v in the y-momentum equation. Hence, a simpler model equation does not seem to be possible. (E.g., replacing y-momentum equation (3.10c) by the boundary-layer equation $\frac{\partial p}{\partial y} = 0$ will make ρ unresolvable already.) From (3.16), it follows as expression for ρ

$$\rho = \rho\left(\overline{u}, \overline{v}, \overline{\mathrm{Re}h}, \theta_1, \theta_2\right) = \frac{e^{\mathrm{i}\theta_1} A_{1,1} A_{3,2}}{A_{1,1}A_{3,2} - A_{1,2}A_{2,1}A_{3,3}}, \tag{3.18}$$

with the $A_{i,j}$'s the elements of the matrix in (3.16). Note that, given relation (3.17), ρ is indeed identical to ρ_3 in (3.14), which confirms the correctness of (3.15).

For analysis purposes, expression (3.18) is still too intricate. To simplify the analysis, $\overline{v}$ is set to zero. (This elimination of $\overline{v}$ does not do much harm to the practical relevance of the analysis, $\overline{v}$ is the least important of the three free parameters.) Then, the corresponding expression for the amplification factor becomes of the remarkably simple form $\rho = \rho\left(\theta_1, \theta_2\right)$. Thus, for $\overline{v} = 0$, the amplification factor depends on the elliptic part only. The expression for the amplification factor (for $\overline{v} = 0$) is

$$\rho = \frac{e^{\mathrm{i}\theta_1}\left(3-4e^{-\mathrm{i}\theta_1}+e^{-2\mathrm{i}\theta_1}\right)}{\left(3-4e^{-\mathrm{i}\theta_1}+e^{-2\mathrm{i}\theta_1}\right)+8\tan^2\left(\frac{\theta_2}{2}\right)}. \tag{3.19}$$

In Figure 4, $|\rho| = |\rho\left(\theta_1, \theta_2\right)|$ according to (3.19) has been plotted. Investigation of (3.19) learns that $|\rho| \leq 1$, $\forall\theta_1, \theta_2$, and that for $\theta_2 = 0$ it reaches its maximum value: $|\rho\left(\theta_1, \theta_2 = 0\right)| = 1, \forall\theta_1$. So, all errors that are constant in the direction normal to the mainstream direction are not removed by the relaxation. In the real (i.e., the non-periodic) PARNASSOS practice, boundary conditions will hamper

the occurrence of most of these ($\theta_2 = 0$)-errors. For the still remaining ($\theta_2 = 0$)-errors, it may be assumed that they are simply convected out of the computational domain (at the outflow boundary) and not fed in at the same rate at inflow. So, these remaining errors may slow down convergence, but they will not stop it. (However, note that the slowing-down may be significant deep down in the boundary layer, where the flow speed is low.) Concerning the suitability of the pressure relaxation for multigrid acceleration, it has to be concluded that this is modest, because of the locally rather large values of $|\rho|$ in the high-frequency domain $(|\theta_1|, |\theta_2|) \in \{[0,\pi] \times [0,\pi] \mid |\theta_1| \in \left[\frac{\pi}{2}, \pi\right] \vee |\theta_2| \in \left[\frac{\pi}{2}, \pi\right]\}$.

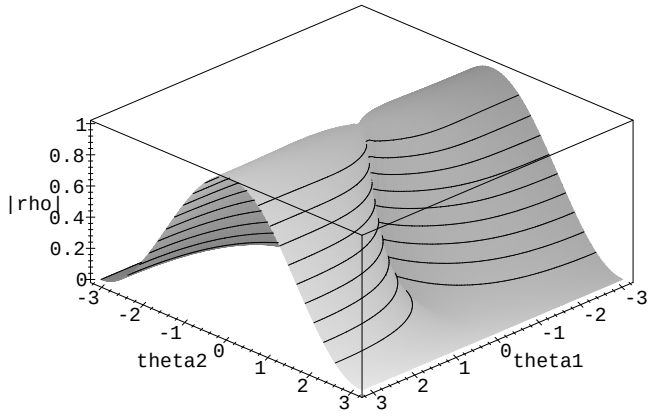

Figure 4: Modulus amplification factor downstream pressure relaxation, $\overline{v} = 0$, existing PARNASSOS discretization.

3.4 Convergence rate

The convergence rate of the complete solution method is determined by that of the outer iteration, the pressure relaxation. To investigate its convergence, we look at

$$u_{i,j}^n \frac{3u_{i,j}^n - 4u_{i-1,j}^n + u_{i-2,j}^n}{2h} + v_{i,j}^n \frac{u_{i,j+1}^n - u_{i,j-1}^n}{2h} + \frac{p_{i+1,j}^{n-1} - p_{i,j}^n}{h} - \frac{1}{\overline{\overline{\mathrm{Re}}}} \frac{u_{i,j+1}^n - 2u_{i,j}^n + u_{i,j-1}^n}{h^2} = 0. \tag{3.20}$$

From (3.20) directly follows the equation for the evolution of $p_{i,j}$:

$$p_{i,j}^n - p_{i,j}^{n-1} = h \left(u_{i,j}^n \frac{3u_{i,j}^n - 4u_{i-1,j}^n + u_{i-2,j}^n}{2h} + v_{i,j}^n \frac{u_{i,j+1}^n - u_{i,j-1}^n}{2h} + \frac{p_{i+1,j}^{n-1} - p_{i,j}^{n-1}}{h} - \frac{1}{\overline{\overline{\mathrm{Re}}}} \frac{u_{i,j+1}^n - 2u_{i,j}^n + u_{i,j-1}^n}{h^2} \right), \tag{3.21}$$

from which it appears that $p_{i,j}$ evolves at fastest linearly with h. So, halving the mesh size slows down convergence by (at least) a factor 2. Full convergence to steady state may be slowed down by an even larger factor. We proceed by investigating the asymptotic convergence rate, making use of expression (3.19) for the amplification factor.

For the ratio between the initial pressure error, say $|\Delta p|^0$, and that after n (downstream) relaxation sweeps, $|\Delta p|^n$, it can be written $\frac{|\Delta p|^n}{|\Delta p|^0} = |\rho|^n$, with ρ the amplification factor. For the number of correct pressure digits m gained in n relaxation sweeps, we write $\frac{|\Delta p|^n}{|\Delta p|^0} = 10^{-m}$ and hence $m \ln 10 = -n \ln |\rho|$. Defining next the convergence rate, R_c, as $R_c \equiv \frac{m \ln 10}{n}$, with the above relation between the amplification factor and the number of correct digits, it can be written as:

$$R_c = -\ln |\rho| \,. \tag{3.22}$$

From the analysis in Section 3.3, it is known that the error modes which are most critical for convergence lie around $\theta_2 = 0$ (Figure 4). Taylor-series expansion around $\theta_2 = 0$ of ρ according to (3.19) yields

$$|\rho| = 1 - \frac{1 - \cos\theta_1}{5 - 3\cos\theta_1}\theta_2^2 + \mathcal{O}\left(\theta_2^3\right) \tag{3.23}$$

and thus, with (3.22) and the definition $\theta_2 \equiv \omega_2 h$:

$$R_c = \frac{1 - \cos\theta_1}{5 - 3\cos\theta_1}\omega_2^2 h^2 + \mathcal{O}(h^3). \tag{3.24}$$

From (3.24), it follows that the method asymptotically converges at an $\mathcal{O}(h^2)$-rate, which is one order slower than the global convergence rate predicted in the beginning of this section. Assuming that the $\mathcal{O}(h^2)$ convergence-rate estimate is also valid in 3D, this means that halving the mesh size in a 3D PARNASSOS situation may lead to a 32 times larger CPU time for full convergence to steady state.

3.5 Conclusions so far

In summary, the following can already be concluded on the existing numerical method. The discretization is almost second-order accurate; only the difference formula for $\frac{\partial p}{\partial x}$ is first-order accurate. Concerning the solution method, the pressure relaxation shows the following property that may ask for some further attention. Good convergence is not guaranteed for all error modes; the pressure relaxation's asymptotic convergence rate may be $\mathcal{O}(h^2)$ only. In the next sections, some possible modifications to PARNASSOS will be investigated.

4. Modifications with no or negative effect expected

4.1 First-order backward differences for $u\frac{\partial u}{\partial x}$ and $u\frac{\partial v}{\partial x}$

To improve the convergence properties of the pressure relaxation, one might start by replacing some higher-order accurate discrete x-derivatives by first-order ones. This may yield better stability and convergence properties without the formal loss of an order of accuracy since the discretization is already first-order accurate. For this replacement, the three-point backward difference formulae applied to the terms $u\frac{\partial u}{\partial x}$ and $u\frac{\partial v}{\partial x}$ are no candidates. Replacement of these difference formulae by first-order accurate ones does not change amplification factor (3.19), since this depends on the elliptic part alone.

4.2 First-order backward difference for $\frac{\partial u}{\partial x}$ in continuity equation

Replacement of the three-point backward difference formula for $\frac{\partial u}{\partial x}$ in the continuity equation, by the two-point backward formula, *is* a possibility. Then, maintaining the staggering in y-direction, instead

of (3.16), one gets

$$\begin{pmatrix} \frac{1}{2}\left(1-e^{-\mathrm{i}\theta_1}\right)\left(1+e^{-\mathrm{i}\theta_2}\right) & 1-e^{-\mathrm{i}\theta_2} & 0 \\ \frac{1}{2}\overline{u}\left(3-4e^{-\mathrm{i}\theta_1}+e^{-2\mathrm{i}\theta_1}\right)+ \\ \frac{1}{2}\overline{v}\left(e^{\mathrm{i}\theta_2}-e^{-\mathrm{i}\theta_2}\right)- \\ \frac{1}{\mathrm{Re}h}\left(e^{\mathrm{i}\theta_2}-2+e^{-\mathrm{i}\theta_2}\right) & 0 & \frac{1}{\rho}e^{\mathrm{i}\theta_1}-1 \\ 0 & \frac{1}{4}\overline{u}\left(3-4e^{-\mathrm{i}\theta_1}+e^{-2\mathrm{i}\theta_1}\right)\left(e^{\mathrm{i}\theta_2}+1\right)+ \\ & \overline{v}\left(e^{\mathrm{i}\theta_2}-1\right)- \\ & \frac{1}{2}\frac{1}{\mathrm{Re}h}\left(e^{\mathrm{i}\theta_2}-2+e^{\mathrm{i}\theta_2}\right)\left(e^{\mathrm{i}\theta_2}+1\right) & e^{\mathrm{i}\theta_2}-1 \end{pmatrix} \begin{pmatrix} u \\ v \\ p \end{pmatrix}_{i,j}^{n} = \begin{pmatrix} 0 \\ 0 \\ 0 \end{pmatrix}, \tag{4.1}$$

leading to a slightly improved amplification factor (Figure 5). So, only a very small improvement of the pressure relaxation's convergence is expected. Given the slightly deteriorated accuracy of the discretization, no net positive effect is anticipated from this discretization.

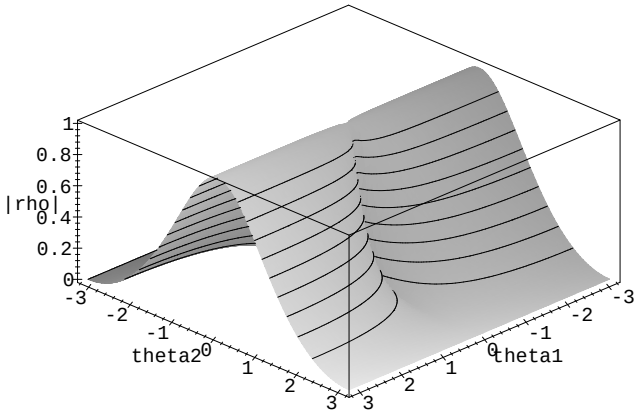

Figure 5: Modulus amplification factor downstream pressure relaxation, $\overline{v}=0$, first-order upstream difference for $\frac{\partial u}{\partial x}$ in continuity equation.

4.3 Second-order central differences for $\frac{\partial u}{\partial x}$ in continuity equation and for $\frac{\partial p}{\partial x}$

In Section 2.1, it has been shown that the continuity equation and the pressure derivatives cause the flow equations to be partly elliptic. In this elliptic part, there is no directional preference. Hence, instead of an upstream discretization of $\frac{\partial u}{\partial x}$ in the continuity equation and a downstream discretization of $\frac{\partial p}{\partial x}$, central discretizations seem to be more natural. A consequence is that, when sticking to plane relaxation, besides $p_{i+1,j}$ (as occurring in the difference formula for $\frac{\partial p}{\partial x}$), one now has two extra downstream unknowns: $u_{i+1,j}$ and $u_{i+1,j-1}$ in the difference formula for $\frac{\partial u}{\partial x}$ in the continuity equation. I.e., in (3.10a), $\frac{1}{4}\left[\left(3u^n_{i,j-1}-4u^n_{i-1,j-1}+u^n_{i-2,j-1}\right)+\left(3u^n_{i,j}-4u^n_{i-1,j}+u^n_{i-2,j}\right)\right]$ is replaced by $\frac{1}{4}\left[\left(u^{n-1}_{i+1,j-1}-u^n_{i-1,j-1}\right)+\left(u^{n-1}_{i+1,j}-u^n_{i-1,j}\right)\right]$. (In (3.10b), $p^{n-1}_{i+1,j}-p^n_{i,j}$ is replaced by $\frac{1}{2}\left(p^{n-1}_{i+1,j}-p^n_{i-1,j}\right)$.) So, for analyzing the convergence of the pressure relaxation, Ansatz (3.15) can

no longer be made. Writing the pressure relaxation again as (3.12a), instead of (3.12b) and (3.12c), we now have

$$L = \begin{pmatrix} \frac{1}{4}\left(e^{\mathrm{i}\theta_1} - e^{-\mathrm{i}\theta_1}\right)\left(1 + e^{-\mathrm{i}\theta_2}\right) & 1 - e^{-\mathrm{i}\theta_2} & 0 \\ \frac{1}{2}\overline{u}\left(3 - 4e^{-\mathrm{i}\theta_1} + e^{-2\mathrm{i}\theta_1}\right) + \frac{1}{2}\overline{v}\left(e^{\mathrm{i}\theta_2} - e^{-\mathrm{i}\theta_2}\right) - \frac{1}{\overline{\mathrm{Re}}h}\left(e^{\mathrm{i}\theta_2} - 2 + e^{-\mathrm{i}\theta_2}\right) & 0 & \frac{1}{2}\left(e^{\mathrm{i}\theta_1} - e^{-\mathrm{i}\theta_1}\right) \\ 0 & \frac{1}{4}\overline{u}\left(3 - 4e^{-\mathrm{i}\theta_1} + e^{-2\mathrm{i}\theta_1}\right)\left(e^{\mathrm{i}\theta_2} + 1\right) + \overline{v}\left(e^{\mathrm{i}\theta_2} - 1\right) - \frac{1}{2}\frac{1}{\overline{\mathrm{Re}}h}\left(e^{\mathrm{i}\theta_2} - 2 + e^{-\mathrm{i}\theta_2}\right)\left(e^{\mathrm{i}\theta_2} + 1\right) & e^{\mathrm{i}\theta_2} - 1 \end{pmatrix} \quad \text{and} \tag{4.2a}$$

$$\tilde{L} = L - \begin{pmatrix} \frac{1}{4}e^{\mathrm{i}\theta_1}\left(1 + e^{-\mathrm{i}\theta_2}\right) & 0 & 0 \\ 0 & 0 & \frac{1}{2}e^{\mathrm{i}\theta_1} \\ 0 & 0 & 0 \end{pmatrix}. \tag{4.2b}$$

From (4.2), it can be seen that as opposed to (3.12), here the amplification matrix $M = \tilde{L}^{-1}\left(\tilde{L} - L\right)$ has only one eigenvalue equal to zero ($\rho_1 = 0$). The two non-zero eigenvalues ρ_2 and ρ_3 are plotted in Figure 6. From the two graphs, it clearly appears that the convergence properties to be expected from this change to central differences are bad.

4.4 Collocation of residuals

A consequence of the staggering of the equations is that for $\overline{v} \neq 0$ the convergence of the relaxation of the elliptic part does not only depend on the discretization of that part, but also on that of the parabolic part and its coefficients (say $\overline{u}, \overline{v}$ and $\overline{\mathrm{Re}}h$). For the standard collocated grid approach, it can be quickly shown that this is not the case. For that purpose, consider again the continuous system (3.1) and for its discretization: (i) an equidistant grid with $\Delta x = \Delta y = h$ and (ii) difference formulae that are arbitrary, except for the facts that downstream influence still occurs through the difference formula for $\frac{\partial p}{\partial x}$ only and that corresponding velocity derivatives in the x- and y-momentum equations are discretized by the identical, non-staggered formulae. Then, applying, just as in PARNASSOS, pressure relaxation through the x-momentum equation, with Fourier analysis through Ansatz (3.15) (which is valid here), instead of (3.16), we get the more general system

$$\begin{pmatrix} u_x(\theta_1) & v_y(\theta_2) & 0 \\ \overline{u}f_x(\theta_1) + \overline{v}f_y(\theta_2) - \frac{1}{\overline{\mathrm{Re}}h}f_{yy}(\theta_2) & 0 & p_x(\rho,\theta_1) \\ 0 & \overline{u}f_x(\theta_1) + \overline{v}f_y(\theta_2) - \frac{1}{\overline{\mathrm{Re}}h}f_{yy}(\theta_2) & p_y(\theta_2) \end{pmatrix} \begin{pmatrix} u \\ v \\ p \end{pmatrix}^n_{i,j} = \begin{pmatrix} 0 \\ 0 \\ 0 \end{pmatrix}. \tag{4.3}$$

In here, $u_x, v_y, p_x, p_y, f_x, f_y$ and f_{yy} denote the (arbitrary) difference formulae. Deriving an expression for the amplification factor ρ, from (4.3), we get

$$p_x(\rho,\theta_1) = \frac{-v_y(\theta_2)p_y(\theta_2)}{u_x(\theta_1)}, \tag{4.4}$$

which confirms that by not applying staggering, for any $\overline{u}, \overline{v}$ and $\overline{\mathrm{Re}}h$, the convergence properties of the relaxation of the elliptic part depend on the discretization of the elliptic terms only, i.e., the velocity derivatives in the continuity equation and the pressure derivatives.

For the derivatives in (4.4), as an example, we take the same difference formulae as in PARNASSOS (apart from the staggering), i.e., in Fourier form:

$$p_x(\rho,\theta_1) = \frac{1}{\rho}e^{\mathrm{i}\theta_1} - 1, \tag{4.5a}$$

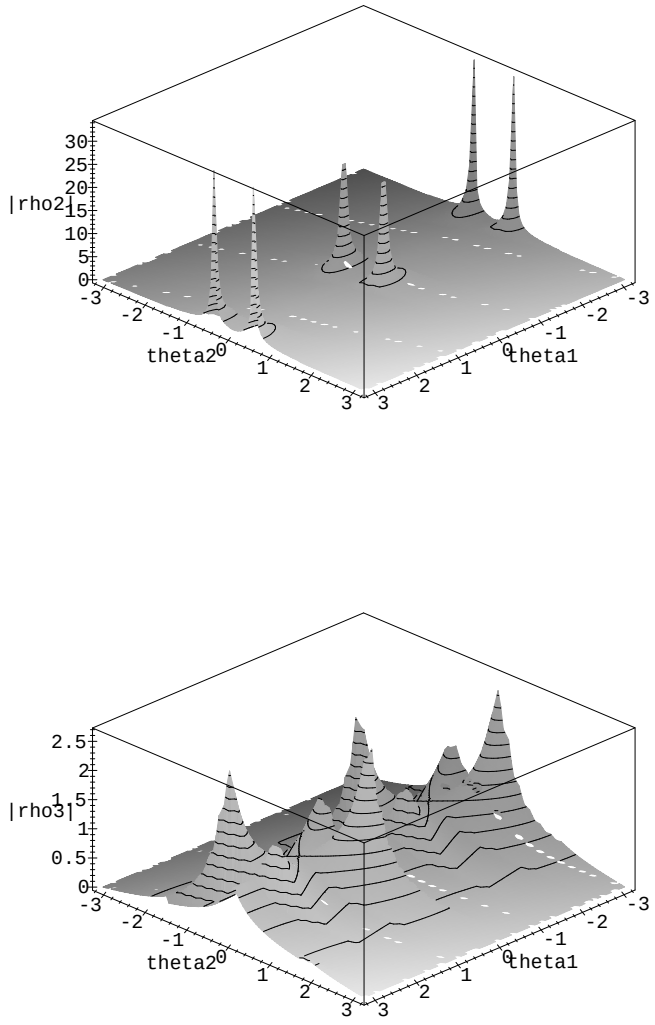

Figure 6: Moduli non-zero eigenvalues amplification matrix downstream pressure relaxation, $\overline{v} = 0$, second-order central differences for $\frac{\partial u}{\partial x}$ in continuity equation and $\frac{\partial p}{\partial x}$.

$$u_x(\theta_1) = \frac{1}{2}\left(3 - 4e^{-\mathrm{i}\theta_1} + e^{-2\mathrm{i}\theta_1}\right), \tag{4.5b}$$

$$v_y(\theta_2) = p_y(\theta_2) = \frac{1}{2}\left(e^{\mathrm{i}\theta_2} - e^{-\mathrm{i}\theta_2}\right). \tag{4.5c}$$

With (4.5), it then follows from (4.4)

$$\rho = \frac{e^{\mathrm{i}\theta_1}\left(3 - 4e^{-\mathrm{i}\theta_1} + e^{-2\mathrm{i}\theta_1}\right)}{(3 - 4e^{-\mathrm{i}\theta_1} + e^{-2\mathrm{i}\theta_1}) + 2\sin^2\theta_2}. \tag{4.6}$$

In Figure 7, $|\rho|$ according to (4.6) has been plotted. Comparing Figure 7 with Figure 4, it has to be concluded that this collocated residual approach is a bad alternative. Thus, in fact, an important motivation has been found for the staggering in y-direction, as it is applied in PARNASSOS.

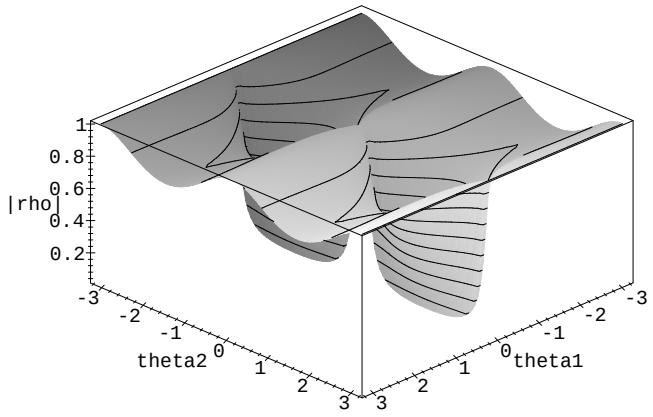

Figure 7: Modulus amplification factor downstream pressure relaxation, collocated (for the remainder: PARNASSOS-discretization).

5. Modifications with unclear effects

5.1 Crank-Nicolson scheme for parabolic part

A widely used discretization method for parabolic partial differential equations is the Crank-Nicolson scheme. Compared to the three-point backward difference formula as applied in PARNASSOS, it has better accuracy and monotonicity properties. This will be shown. An important difference is that it is more compact. The greater compactness implies self-startingness and – maybe – a smaller sensitivity to grid irregularities in flow direction. We make analyses of the accuracy, monotonicity and stability on the basis of model equation (3.4). Considering again an equidistant grid with $\Delta x = \Delta y = h$, for $\overline{u} > 0$, the Crank-Nicolson discretization of (3.4) yields

$$\overline{u}\frac{u_{i,j} - u_{i-1,j}}{h} - \frac{1}{2}\frac{1}{\mathrm{Re}}\frac{(u_{i,j+1} - 2u_{i,j} + u_{i,j-1}) + (u_{i-1,j+1} - 2u_{i-1,j} + u_{i-1,j-1})}{h^2} = 0, \quad \overline{u} > 0. \tag{5.1}$$

The corresponding modified equation in point i,j is

$$\left(1-\frac{h}{2}\frac{\partial}{\partial x}+\frac{h^2}{4}\frac{\partial^2}{\partial x^2}\right)\left(\overline{u}\frac{\partial u}{\partial x}-\frac{1}{\overline{\mathrm{Re}}}\frac{\partial^2 u}{\partial y^2}\right)-\frac{h^2}{12}\left(\overline{u}\frac{\partial^3 u}{\partial x^3}+\frac{1}{\overline{\mathrm{Re}}}\frac{\partial^4 u}{\partial y^4}\right)=\mathcal{O}(h^3), \tag{5.2}$$

which boils down to

$$\overline{u}\frac{\partial u}{\partial x}-\frac{1}{\overline{\mathrm{Re}}}\frac{\partial^2 u}{\partial y^2}=\frac{h^2}{12}\left(\overline{u}\frac{\partial^3 u}{\partial x^3}+\frac{1}{\overline{\mathrm{Re}}}\frac{\partial^4 u}{\partial y^4}\right)+\mathcal{O}(h^3). \tag{5.3}$$

For the three-point backward difference formula, the corresponding modified equation is

$$\overline{u}\frac{\partial u}{\partial x}-\frac{1}{\overline{\mathrm{Re}}}\frac{\partial^2 u}{\partial y^2}=\frac{h^2}{4}\left(-\overline{u}\frac{\partial^3 u}{\partial x^3}+\frac{1}{6}\frac{1}{\overline{\mathrm{Re}}}\frac{\partial^4 u}{\partial y^4}\right)+\mathcal{O}(h^3). \tag{5.4}$$

So, for the very high-Reynolds number flows occurring in ship hydrodynamics, the Crank-Nicolson scheme is expected to yield more accurate results.

As far as the monotonicity of the Crank-Nicolson scheme is concerned, from (5.1) it follows

$$u_{i,j}=\frac{\left(1-\frac{1}{\overline{u}\overline{\mathrm{Re}}h}\right)u_{i-1,j}+\frac{1}{2}\frac{1}{\overline{u}\overline{\mathrm{Re}}h}\left(u_{i,j+1}+u_{i,j-1}+u_{i-1,j+1}+u_{i-1,j-1}\right)}{1+\frac{1}{\overline{u}\overline{\mathrm{Re}}h}},\quad \overline{u}>0, \tag{5.5}$$

which guarantees monotonicity if $\overline{u}>\frac{1}{\overline{\mathrm{Re}}h}$. For the three-point backward difference formula, there is no guarantee at all for monotonicity (Section 3.2).

A known deficiency of the Crank-Nicolson scheme is that it has a poor damping of high-frequency errors, see, e.g., [5], p. 69, [4], p. 241 and [7], p. 429. We verify the stability properties of the Crank-Nicolson scheme. Consider again a grid with $\Delta x=\Delta y=h$ and the Fourier form (3.7). Substitution of this form into (5.1) yields as expression for the amplification factor ρ

$$\rho=\frac{1-\alpha}{1+\alpha},\quad \alpha=\frac{2}{\overline{u}\overline{\mathrm{Re}}h}\sin^2\left(\frac{\theta_2}{2}\right),\quad \overline{u}>0. \tag{5.6}$$

The stability requirements $-1\leq\rho\leq 1$ are satisfied for all $\overline{u}\overline{\mathrm{Re}}h$, $\overline{u}>0$ and all θ_2. However, it holds $\lim_{\overline{u}\overline{\mathrm{Re}}h\downarrow 0}\rho\left(\theta_2=\pm\pi\right)=-1$. So, high-frequency errors (in j-direction), in the limit $\overline{u}\overline{\mathrm{Re}}h\downarrow 0$, appear to be neutrally stable.

Particularly because of its greater compactness (and thus its smaller sensitivity to strong grid irregularities), the Crank-Nicolson scheme might be an interesting alternative for the three-point backward scheme. When striving for overall compactness, the discretization of, e.g., the $\frac{\partial u}{\partial x}$-term in the continuity equation needs to be reconsidered as well.

5.2 Alternative pressure boundary conditions at outflow

In PARNASSOS, a Neumann condition for the pressure is imposed at the outflow boundary, $\frac{\partial p}{\partial n}=0$. To suppress the downstream exponential solution growth found in Section 2.2, a Dirichlet condition is much more effective than a Neumann condition. On the other hand, a Dirichlet condition may behave worse than a Neumann condition with respect to the reflection of iteration errors. Instead of $\frac{\partial p}{\partial n}=0$, one may also take the presumably even less reflective condition $\frac{\partial p}{\partial n}=\frac{\partial p}{\partial x}=-u\frac{\partial u}{\partial x}-v\frac{\partial u}{\partial y}-w\frac{\partial u}{\partial z}+\frac{1}{\mathrm{Re}}\left(\frac{\partial^2 u}{\partial y^2}+\frac{\partial^2 u}{\partial z^2}\right)$, where the terms in the righthand side can be extrapolated from the interior flow domain. A mixed (Robin) boundary condition is also a possibility.

6. Modifications with expected positive effects

6.1 Underrelaxation of the elliptic part

In the present section, it will be investigated whether under- or overrelaxation can improve the convergence properties of the pressure relaxation, as found in Section 3.3. Consider the plain relaxation

formula (3.10b) in the rewritten form

$$\frac{1}{2}\overline{u}\left(3u^n_{i,j}-4u^n_{i-1,j}+u^n_{i-2,j}\right)+\frac{1}{2}\overline{v}\left(u^n_{i,j+1}-u^n_{i,j-1}\right)+\left(p^{n-1}_{i+1,j}-p^{n-1}_{i,j}\right)+\left(p^{n-1}_{i,j}-p^n_{i,j}\right)-\frac{1}{\overline{\mathrm{Re}}h}\left(u^n_{i,j+1}-2u^n_{i,j}+u^n_{i,j-1}\right)=0 \quad (6.1)$$

and introduce as the pressure correction $\tilde{p}^n_{i,j}-p^{n-1}_{i,j}$ to be accepted:

$$\tilde{p}^n_{i,j}-p^{n-1}_{i,j}=\omega\left(p^n_{i,j}-p^{n-1}_{i,j}\right), \quad (6.2)$$

with ω the relaxation factor and $p^n_{i,j}-p^{n-1}_{i,j}$ the pressure correction following from plain relaxation formula (3.10b). Substituting (6.2) into (6.1) and dropping the ˜ on $\tilde{p}^n_{i,j}$, instead of (3.10b), we get its under- or overrelaxation version

$$\frac{1}{2}\overline{u}\left(3u^n_{i,j}-4u^n_{i-1,j}+u^n_{i-2,j}\right)+\frac{1}{2}\overline{v}\left(u^n_{i,j+1}-u^n_{i,j-1}\right)+\left[p^{n-1}_{i+1,j}-\left(\frac{1}{\omega}p^n_{i,j}+\left(1-\frac{1}{\omega}\right)p^{n-1}_{i,j}\right)\right]-\frac{1}{\overline{\mathrm{Re}}h}\left(u^n_{i,j+1}-2u^n_{i,j}+u^n_{i,j-1}\right)=0. \quad (6.3)$$

Maintaining (3.10a) and (3.10c) and taking again the Ansatz (3.15), instead of (3.16), we get the system

$$\begin{pmatrix} \frac{1}{4}\left(3-4e^{-\mathrm{i}\theta_1}+e^{-2\mathrm{i}\theta_1}\right)\left(1+e^{-\mathrm{i}\theta_2}\right) & 1-e^{-\mathrm{i}\theta_2} & 0 \\ \frac{1}{2}\overline{u}\left(3-4e^{-\mathrm{i}\theta_1}+e^{-2\mathrm{i}\theta_1}\right)+\frac{1}{2}\overline{v}\left(e^{\mathrm{i}\theta_2}-e^{-\mathrm{i}\theta_2}\right)-\frac{1}{\overline{\mathrm{Re}}h}\left(e^{\mathrm{i}\theta_2}-2+e^{-\mathrm{i}\theta_2}\right) & 0 & \frac{1}{\rho}e^{\mathrm{i}\theta_1}-\left(\frac{1}{\omega}+\left(1-\frac{1}{\omega}\right)\frac{1}{\rho}\right) \\ 0 & \frac{1}{4}\overline{u}\left(3-4e^{-\mathrm{i}\theta_1}+e^{-2\mathrm{i}\theta_1}\right)\left(e^{\mathrm{i}\theta_2}+1\right)+\overline{v}\left(e^{\mathrm{i}\theta_2}-1\right)-\frac{1}{2}\frac{1}{\overline{\mathrm{Re}}h}\left(e^{\mathrm{i}\theta_2}-2+e^{-\mathrm{i}\theta_2}\right)\left(e^{\mathrm{i}\theta_2}+1\right) & e^{\mathrm{i}\theta_2}-1 \end{pmatrix}\begin{pmatrix} u \\ v \\ p \end{pmatrix}^n_{i,j}=\begin{pmatrix} 0 \\ 0 \\ 0 \end{pmatrix}. \quad (6.4)$$

For $\overline{v}=0$, it follows from (6.4) as expression for the amplification factor

$$\rho=\frac{\left(\omega\left(e^{\mathrm{i}\theta_1}-1\right)+1\right)\left(3-4e^{-\mathrm{i}\theta_1}+e^{-2\mathrm{i}\theta_1}\right)}{\left(3-4e^{-\mathrm{i}\theta_1}+e^{-2\mathrm{i}\theta_1}\right)+8\omega\tan^2\left(\frac{\theta_2}{2}\right)}. \quad (6.5)$$

For the $\omega=1$-relaxation case, in Section 3.3, we already saw that it is neutrally stable for errors that are constant in j-direction. From (6.5), it is derived

$$|\rho\left(\omega,\theta_1,\theta_2=0\right)|=\sqrt{1+2\omega(\omega-1)(1-\cos\theta_1)}, \quad (6.6)$$

from which it appears that underrelaxation is convergent for all ($\theta_2=0$)-errors, except for the ($\theta_1=\theta_2=0$)-error, which forms no problem since it is supposed to be absent in case of boundary conditions. From (6.6), it also appears that the best result is obtained for $\omega=\frac{1}{2}$. In Figure 8, the amplification factor's modulus for $\omega=\frac{1}{2}$ has been plotted over the complete frequency domain. Comparison with the graph for the plain relaxation (Figure 4) clearly shows the positive effect of the underrelaxation with $\omega=\frac{1}{2}$. Particularly interesting is that it has significantly better smoothing properties than plain relaxation.

Convergence rate. Analogous to pressure evolution formula (3.21), for underrelaxation it can be derived the formula

$$p^n_{i,j}-p^{n-1}_{i,j}=\omega h\left(u^n_{i,j}\frac{3u^n_{i,j}-4u^n_{i-1,j}+u^n_{i-2,j}}{2h}+v^n_{i,j}\frac{u^n_{i,j+1}-u^n_{i,j-1}}{2h}+\frac{p^{n-1}_{i+1,j}-p^{n-1}_{i,j}}{h}-\frac{1}{\overline{\mathrm{Re}}}\frac{u^n_{i,j+1}-2u^n_{i,j}+u^n_{i,j-1}}{h^2}\right). \quad (6.7)$$

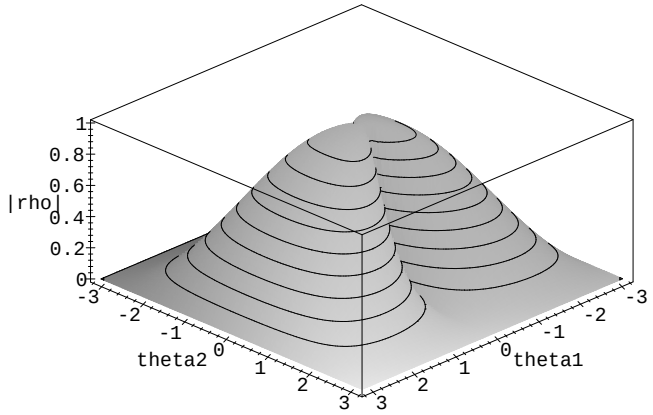

Figure 8: Modulus amplification factor downstream pressure relaxation, $\overline{v} = 0$, existing PARNASSOS discretization, underrelaxation with $\omega = \frac{1}{2}$.

So, from (6.7) it appears that $p_{i,j}$ still evolves at fastest linearly with h. As in Section 3.4, we also consider the asymptotic convergence rate. From Figure 8, it is seen that the errors which are most critical for the asymptotic convergence rate lie around $\theta_1 = \theta_2 = 0$. For $\omega = \frac{1}{2}$, Taylor-series expansion of (6.5) around $\theta_1 = \theta_2 = 0$ yields (using expression (3.22) together with the definitions $\theta_1 \equiv \omega_1 h$ and $\theta_2 \equiv \omega_2 h$):

$$R_c = \frac{1}{8}\frac{\omega_1^4 + \omega_2^4}{\omega_1^2}h^2 + \mathcal{O}(h^3). \tag{6.8}$$

So, also for underrelaxation with the optimal value $\omega = \frac{1}{2}$, the asymptotic convergence rate is still $\mathcal{O}(h^2)$ only. Fortunately, good multigrid acceleration seems to be attainable. In the ideal case, this leads to grid-independent (i.e., $\mathcal{O}(h^0)$) convergence rates.

6.2 Linearization of the parabolic part

The nonlinearity in the reduced, continuous Navier-Stokes equations is present in the parabolic part only, in 3D turbulent practice: through the coefficients u, v, w and $\frac{1}{\mathrm{Re}}$. In PARNASSOS, at each i-station, the corresponding discrete nonlinear system (with coefficients $u_{i,j,k}, v_{i,j,k}, w_{i,j,k}$ and $\frac{1}{\mathrm{Re}_{i,j,k}}$) is solved through a Newton technique. The discrete nonlinear system can be simply linearized (without reducing its order of accuracy), by replacing the above coefficients by their second-order accurate extrapolants from backward sweep direction. For the downstream and upstream relaxation sweep, respectively, these extrapolants are

$$q_{i,j,k} = 2q_{i-1,j,k} - q_{i-2,j,k}, \tag{6.9a}$$

$$q_{i,j,k} = 2q_{i+1,j,k} - q_{i+2,j,k}, \tag{6.9b}$$

with $q \equiv (u, v, w, \mathrm{Re})$. (Note that this higher-order extrapolation of the nonlinear coefficients does not combine that well with the Crank-Nicolson scheme; it undoes its compactness.)

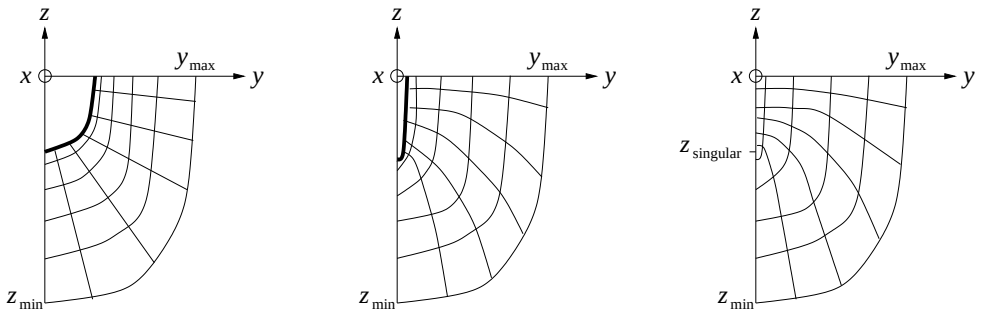

a. Around non-slender hull. b. Around slender hull. c. Downstream of hull.

Figure 9: O-type grid planes around half-hull cross sections.

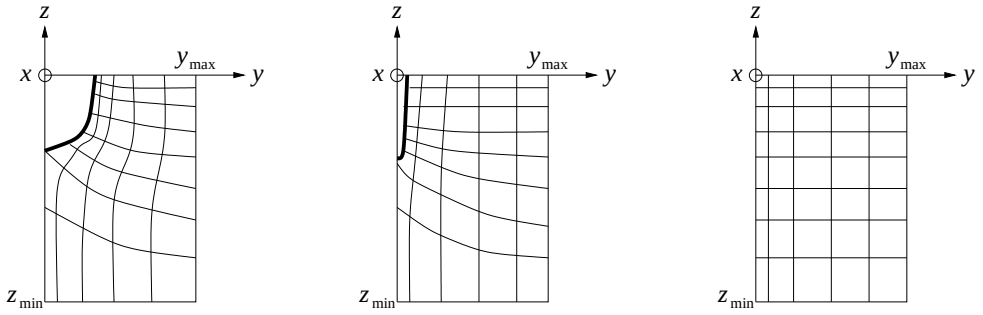

a. Around non-slender hull. b. Around slender hull. c. Downstream of hull.

Figure 10: H-type grid planes around half-hull cross sections.

6.3 HH-type grid

As already seen in Section 1.2, where the hull cross sections are not slender and free of corners, an O-type grid plane is a good choice (Figure 9a). However, the more slender the hull's cross section is, the less regular the grid plane is (Figure 9b). In the wake, the O-type grid plane contains a genuine singularity. Now, a fix to the ship-stern singularity may be to take an H-type grid at the present planes as well. This leads to a more regular, though, not yet perfectly regular grid: in case of the non-slender hull cross section (Figure 10a), the grid line along the hull shows a kink at the ship's symmetry plane. However, behind the ship (Figure 10c) and maybe also at the ship stern itself, the grid is perfectly regular. As opposed to the HO-type grid from Section 1.2, the present resulting HH-type grid will normally give a computational domain with rectilinear farfield boundaries only (Figure 11), say a cube-type instead of a cylinder-type domain (Figure 1). Besides the cube-type and cylinder-type domain, the possibility of a sphere-type domain still exists (Figure 12). The natural grid in the latter domain is of OO-type, with as natural direction for the polar axis the z-direction. Unfortunately, such a regular grid is no good option for the reduced Navier-Stokes equations (for full Navier-Stokes equations, it may be so), because in the ship-stern region, the mainstream flow will not be grid-aligned. There, it will switch from circumferential to radial direction. In conclusion, the OO-type grid type is no alternative grid type which is already worth to be investigated, the HH-type on the contrary, *is*.

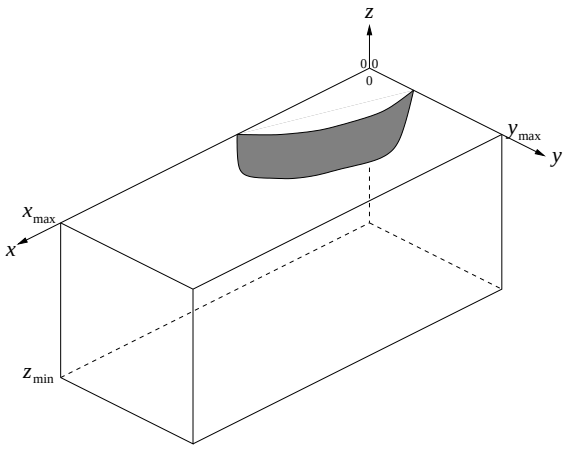

Figure 11: Cube-type computational domain.

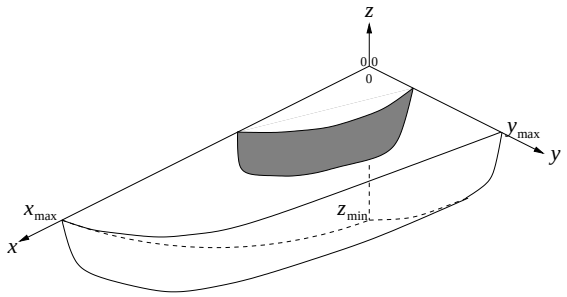

Figure 12: Sphere-type computational domain.

7. Conclusions

Of the promising modifications proposed to the solution method for the *elliptic part* of the reduced Navier-Stokes equations, the simplest is downstream underrelaxation with $\omega = \frac{1}{2}$. It is particularly promising because it has good error-smoothing properties and – thus – good multigrid-acceleration properties. (It has not yet been investigated whether the ($\omega = \frac{1}{2}$) downstream underrelaxation is appropriate for fully second-order accurate discrete equations as well.) In numerical experiments with alternative numerical techniques for the elliptic part, it may be worthwhile to investigate the effect of a Dirichlet (or mixed) condition for the pressure at outflow, instead of the existing homogeneous Neumann condition.

For the solver of the *parabolic part* of the equations, it may be interesting: (i) to linearize it (by second-order accurate extrapolation in backward sweep direction), or (ii) to replace the three-point backward difference scheme by the Crank-Nicolson scheme. The Crank-Nicolson scheme is more compact in flow direction and – therefore – possibly less sensitive to grid irregularities in flow direction. (Use of the Crank-Nicolson scheme for reasons of compactness excludes the second-order accurate linearization.)

With respect to the *grid*, it may be worth the effort to use an HH-type grid instead of an HO-type grid. This replacement may remove the grid singularity.

The suggested modifications can be combined in various ways.

Acknowledgement
The author thanks Martin Hoekstra for his suggestions to improve this report.

References

1. A.J. Chorin, A numerical method for solving incompressible viscous flow problems *Journal of Computational Physics*, **2**, 12–26 (1967).
2. M. Van Dyke, *Perturbation Methods in Fluid Mechanics* (The Parabolic Press, Stanford, 1975).
3. D. Dijkstra, The solution of the Navier-Stokes equations near the trailing edge of a flat plate, PhD-thesis (State University of Groningen, Groningen, 1974).
4. C.A.J. Fletcher, *Computational Techniques for Fluid Dynamics, Volume I: Fundamental and General Techniques* (Springer, New York, 1988).
5. B. Gustafsson, H.O. Kreiss and J. Oliger, *Time Dependent Problems and Difference Methods* (Wiley, New York, 1995).
6. F.H. Harlow and J.E. Welch, Numerical calculation of time-dependent viscous incompressible flow of fluid with free surface, *Physics of Fluids*, **2**, 2182–2189 (1965).
7. Ch. Hirsch, *Numerical Computation of Internal and External Flows, Volume I: Fundamentals of Numerical Discretization* (Wiley, New York, 1995).
8. M. Hoekstra, Computation of steady viscous flow near a ship's stern, in: P. Wesseling, Ed., *Research in Numerical Fluid Mechanics*, *Notes on Numerical Fluid Mechanics*, **17**, 45–57 (Vieweg, Braunschweig, 1987).
9. M. Hoekstra and H.C. Raven, Ship boundary-layer and wake calculations with a parabolised Navier-Stokes solution system, in *Proceedings Fourth International Conference on Numerical Ship Hydrodynamics*, Washington, D.C. (1985).
10. M. Hoekstra and H.C. Raven, Application of a parabolised Navier-Stokes solution system to ship stern flow computation, in *Osaka International Colloquium on Ship Viscous Flow*, Osaka (1985).
11. H.C. Raven and M. Hoekstra, A parabolised Navier-Stokes solution method for ship stern flow calculations, in *Proceedings Second International Symposium on Ship Viscous Resistance*, Göteborg (1985).
12. R.D. Richtmyer and K.W. Morton, *Difference Methods for Initial-Value Problems* (Wiley, New York, 1967).
13. K. Stewartson, On the flow near the trailing edge of flat plate II, *Mathematika*, **16**, 106–121 (1969).

Table of Contents